

Line Detection Using A Spatial Characteristic Model

Sheng Liu †, Charles F. Babbs ‡, and Edward J. Delp* †

†Video and Image Processing Laboratory (*VIPER*)

School of Electrical and Computer Engineering

‡Department of Basic Medical Sciences

School of Veterinary Medicine

Purdue University

West Lafayette, Indiana 47907

Corresponding Author:

Professor Edward J. Delp

School of Electrical and Computer Engineering

1285 Electrical Engineering Building

Purdue University

West Lafayette, IN 47907-1285

USA

Telephone: +1 765 494 1740

Fax: +1 765 494 0880

Email: ace@ecn.purdue.edu

Abstract

Line or linear structure detection is a very basic, yet important problem in image processing and computer vision. Many line detection algorithms are based on edge detection and consider lines as extended or contiguous edges. Most techniques require that a binary edge map be first extracted from the image before line detection is performed. In this paper, we propose a new line detection technique that is based on a model that describes spatial characteristics of line structures in an image. This line model uses simple properties of lines that include both graylevel and geometric features. The performance of the line detector on natural scenes and medical images will be shown. The technique is shown to be capable of detecting lines of different width, lines of varying width, as well as curves.

Index Terms: line detection, curve detection, edge detection, image analysis.

EDICS: IP 2-ANAL or 2-NFLT

This work was supported by a grant from the National Institutes of Health, Grant Number CA62243, and a fellowship from the Purdue Cancer Center.

1 Introduction

Line or linear structure detection is a very basic, yet important problem in image processing and computer vision. It is often the preprocessing step in other applications such as object recognition and tracking. Lines are commonly viewed as extended or contiguous edges. Consequently, many line detection algorithms extract local edges first, then group them into lines. For example, Nevatia and Babu [1] used edge positions and orientations to link edges; Lee and Kweon [2] developed a six-step algorithm that consists of, after edge extraction, edge scanning, edge normalization, line-blob extraction, line-feature computation, and line linking; Zucker, *et al* [3] used a relaxation process to group edges into lines; Kanazawa and Kanatani [4] used an asymptotic approximation to fit a model of a line to an edge segment; Eichel and Delp [5] used a sequential model to link edge pixels based on Markov random fields. This work was extended to multiresolution approaches by Cook and Delp [6, 7]. Other approaches have also been reported in the literature [8, 9, 10]. The use of local edge operators to first enhance the image usually also enhances noise and tends to generate dense edge maps, which makes subsequent processing difficult [11]. Furthermore, these methods do not respond well to thick lines because pixels in the middle of a thick line are not edge pixels. We will show examples of these problems in Section 2.

Another approach is to parameterize potential lines in edges detected in the scene and then base the detection in the parameter space. The Hough transform [12, 13, 14, 15, 16] has been widely used for detecting lines in binary images using this approach. Suppose there is a line at a distance s and orientation θ , it can be represented as $s = x \cos \theta + y \sin \theta$ for constants s and θ . The Hough transform maps all the pixels on this line into one point in the (s, θ) parameter space. By accumulating the (s, θ) pairs one can use this approach to detect lines. A problem with the Hough transform is that it is not suitable for direct use

in grayscale images (Grayscale extension has been proposed by Lo and Tsai [17]). It also requires preprocessing steps (edge detection and thresholding) to obtain the binary pattern. In addition, the Hough transform does not provide the actual position of the line [18]. This is not sufficient for many applications.

We propose a novel line or linear structure detection technique for grayscale images. This line detector is based on a spatial characteristic model of lines. It is capable of extracting lines with different width, lines with irregular width, as well as curves. In Section 2, we describe this new line model in detail. In Section 3, we present the detection algorithm as well as some implementation issues. Finally, we present experimental results and discussions in Section 4.

2 Spatial Characteristic Model For Lines

Lines are commonly considered as extended or contiguous edges while edges are usually defined as local discontinuity in image graylevels. Therefore, many line detectors are based on gradients. For example, the compass gradient operators [12] shown in Table 1 estimate the graylevel gradients at each pixel location in a number of directions corresponding to the operators. The “orientation” of the pixel at that location corresponds to the operator with the maximum response. This oriented gradient response can then be thresholded to obtain a line detection.¹ Note that the compass operator detects only one pixel wide lines. However, pixels in the middle of a “thick” line do not possess the properties that characterize an edge pixel. (Here, “thick” line refers to a line that has more than 2 pixels in width.) Figure 1 (a) shows a “thin” white line of 1 pixel in width at the top and a “thick” white line of 10 pixels in width at the bottom. Part of the “thick” line is enlarged and shown in Figure 1

¹The compass gradient method described here is prototypical of edge based approaches to line detection and will be used to compare the performance of our proposed method.

(b). It is obvious that an edge operator would not indicate that the shaded pixel in the box in Figure 1 (b) is an edge pixel, even when it operates in a neighborhood as large as the 9×9 window. This is because this 9×9 window is in an uniform region. It is therefore not surprising that line detectors based on edge detection do not respond well to thick lines. As an example, we use the E-W compass gradient operator, as shown in Table 1 (a), on the image in Figure 1 (a). The result is shown in Figure 2. As expected, we see that only the “edges” of the lines are detected.

We propose that one basic characteristic of a line, regardless of its thickness, is that pixels in the line all have similar graylevels. In other words, if a pixel belongs to a line, then there exists a string of pixels along the direction of the line that contains this pixel and have similar graylevels. The term “string” will be used to refer to a single pixel wide line throughout this paper. Lines therefore consist of strings. This is illustrated in Figure 3, where a 3 pixel wide line at 45° is shown. The boxed string of pixels along 45° has the same graylevels as that of the center pixel, which makes the center pixel part of the line. The same idea describes the lines at 0° , 11.25° , 22.5° , and 33.75° , respectively, shown in Figure 4 (a), (b), (c), and (d). Another condition for a line is that its surrounding region has different graylevels from those pixels in the line. In the extreme case of an uniform region, as shown in Figure 5 (a), there are strings of pixels with the same graylevels along any direction, while no line will be seen. Finally, the length of a line is greater than its width. For example, we do not call the bright region in Figure 5 (b) a line.

In summary, our line model is as follows:

1. There is a string of pixels with similar graylevels along a certain direction.
2. The surrounding pixels have different graylevels.
3. The length of a line is greater than its width.

3 Detection Algorithm

As described above, the basic characteristic of a line is that pixels on it have similar graylevels. A measure of graylevel similarity among pixels is the standard deviation. Let (i, j) be the spatial location in the image at row i and column j ; $f(i, j)$ be the pixel graylevel at (i, j) ; $L_{(i,j)}(\theta, l)$ be a string of pixels centered at (i, j) , in direction θ , and of Euclidean length l ; and $N_{L_{(i,j)}(\theta,l)}$ be the integer number of pixels within $L_{(i,j)}(\theta, l)$. Note that $N_{L_{(i,j)}(\theta,l)}$ is different from the length l if the line is not horizontal or vertical. For example, a string in the direction 45° has about $1/\sqrt{2}$ the number of pixels as a string in the direction 0° of the same length, as shown in Figure 6 ². Then the standard deviation of pixel graylevels in $L_{(i,j)}(\theta, l)$ is

$$\sigma_{(i,j)}(\theta, l) = \sqrt{\frac{1}{N_{L_{(i,j)}(\theta,l)} - 1} \sum_{(m,n) \in L_{(i,j)}(\theta,l)} (f(m, n) - \bar{f}_{L_{(i,j)}(\theta,l)})^2}$$

where $(m, n) \in L_{(i,j)}(\theta, l)$ when the string $L_{(i,j)}(\theta, l)$ contains the pixel (m, n) and $\bar{f}_{L_{(i,j)}(\theta,l)}$ is the average graylevel of $L_{(i,j)}(\theta, l)$

$$\bar{f}_{L_{(i,j)}(\theta,l)} = \frac{1}{N_{L_{(i,j)}(\theta,l)}} \sum_{(m,n) \in L_{(i,j)}(\theta,l)} f(m, n)$$

There are $N_{L_{(i,j)}(\theta,l)}$ number of strings passing through (i, j) for given θ and l . An example with $\theta = 0$ and $l = 5$ is shown in Figure 7. Among all the strings that pass through (i, j) in direction θ and of Euclidean length l , we denote their minimum standard deviation as $\gamma^{(i,j)}(\theta, l) = \min_{(m,n) \in L_{(i,j)}(\theta,l)} \{\sigma_{(m,n)}(\theta, l)\}$, and the corresponding string as $L_{\gamma^{(i,j)}(\theta,l)}$. If pixel (i, j) belongs to a line in the direction θ and of length greater than l , then $\gamma^{(i,j)}(\theta, l)$ is small. In the case of an ideal line where all pixels on it have the same graylevels, $\gamma^{(i,j)}(\theta, l) = 0$. Note that l is not the length of the line, but the *minimum* length. It can also be interpreted

²We are assuming that the image is represented on a square grid of pixels.

as the maximum width of the line. We will discuss this below.

Finding a small $\gamma^{(i,j)}(\theta, l)$ does not lead to the conclusion that (i, j) belongs to a line. As illustrated in Figure 5 (a), (i, j) may lie in an uniform region. However, if (i, j) is in an uniform region, then $\gamma^{(i,j)}(\theta, l)$ is small for all θ . Figure 8 (b), (c), and (d) compares the relationship between $\gamma^{(i,j)}(\theta, l)$ and θ for pixels on the thin line, in the background, and on the thick line, respectively, using the image shown in Figure 1 (a) and repeated in Figure 8 (a). If we obtain the standard deviation of $\gamma^{(i,j)}(\theta, l)$ with regard to θ and denote

$$\sigma_{\gamma^{(i,j)}}^2(l) = \int_0^{2\pi} \{(\gamma^{(i,j)}(\theta, l) - \bar{\gamma}^{(i,j)}(l))^2 \frac{1}{2\pi}\} \partial\theta \quad (1)$$

where

$$\bar{\gamma}^{(i,j)}(l) = \int_0^{2\pi} \{\gamma^{(i,j)}(\theta, l) \frac{1}{2\pi}\} \partial\theta \quad (2)$$

Then $\sigma_{\gamma^{(i,j)}}(l)$ is small for the case that (i, j) lies in an uniform region. For the ideal uniform region, $\sigma_{\gamma^{(i,j)}}(l) = 0$ as shown in Figure 8 (c).

l is taken to be 15 in the above comparison. As mentioned earlier, l is actually the maximum width of the lines we want to detect. Note that the black uniform regions in Figure 8 (a) can also be seen as very thick lines. Because we set $l = 15$, which is smaller than the widths of the “black thick lines”, $\gamma^{(i,j)}(\theta, l) = 0$ for all θ and consequently $\sigma_{\gamma^{(i,j)}}(l) = 0$ for (i, j) in the black regions. Remember that the thick white line at the bottom is 10 pixel in width, so if we set $l < 10$, we would have $\sigma_{\gamma^{(i,j)}}(l) = 0$ for (i, j) on this line as well. Therefore, small $\sigma_{\gamma^{(i,j)}}(l)$ indicates an uniform region only when the lines we want to detect have widths smaller than l . This complies with the third characteristic in our line model that the length of a line is larger than its width.

Based on the above analysis, our line detector can be summarized in the block diagram shown in Figure 9. Given an input image I and the minimum length or maximum width of the

lines one wants to detect l , we decide for each pixel (i, j) in the image whether it is on a line or not, and if it is, the orientation of the line. First, for a certain orientation θ , we examine all possible strings of length l that pass through (i, j) , which is $L_{(m,n)}(\theta, l)$ for $\forall(m, n) \in L_{(i,j)}(\theta, l)$. This can be seen from Figure 7. Then for each $L_{(m,n)}(\theta, l)$, find its pixel graylevel standard deviation $\sigma_{(m,n)}(\theta, l)$. Take $\gamma^{(i,j)}(\theta, l) = \min_{(m,n) \in L_{(i,j)}(\theta, l)} \{\sigma_{(m,n)}(\theta, l)\}$. A smaller $\gamma^{(i,j)}(\theta, l)$ indicates a higher probability that (i, j) is on a line in direction θ and of length greater or equal to l . Next for all orientations θ , obtain $\sigma_{\gamma^{(i,j)}}(l)$, $\gamma^{(i,j)}(l) = \min_{\theta} \{\gamma^{(i,j)}(\theta, l)\}$, and denote the corresponding θ as $\theta(i, j)$. A decision can then be made based on $\sigma_{\gamma^{(i,j)}}(l)$ and $\gamma^{(i,j)}(l)$. A smaller $\gamma^{(i,j)}(l)$ and larger $\sigma_{\gamma^{(i,j)}}(l)$ indicates higher probability of a pixel (i, j) belonging to a line, and $\theta(i, j)$ indicates the orientation of the line.

Since the only restriction is the maximum line width, this line detector is capable of detecting

- lines of different width, from single pixel wide up to l
- lines of any length that is longer than l
- lines with varying width, provided that the changes are “slower” than l
- curves, provided that over short segment, they can be approximated as lines of length greater than l

Experimental results in Section 4 will demonstrate these capabilities.

In the actual implementation, it is not necessary to find at every pixel location (i, j) all the strings that pass through this pixel and its corresponding standard deviation in order to obtain $\gamma^{(i,j)}(\theta, l)$. This would be computationally intensive. As illustrated in Figure 7, for any given θ and l , there are $N_{L_{(i,j)}(\theta, l)}$ number of strings passing through the pixel (i, j) . Instead, we only need to consider one string for each pixel (i, j) , such as $L_{(i,j)}(\theta, l)$ that

centers at (i, j) . The steps to obtain $\gamma^{(i,j)}(\theta, l)$ are as follows:

- Initialize $\gamma^{(i,j)}(\theta, l)$ to a large value for every pixel (i, j) in the image.
- For each row i and each column j
 1. For the pixel (i, j) , obtain $\sigma_{(i,j)}(\theta, l)$
 2. Compare this $\sigma_{(i,j)}(\theta, l)$ to every $\gamma^{(m,n)}(\theta, l)$, for $\forall(m, n) \in L_{(i,j)}(\theta, l)$.
 3. Replace $\gamma^{(m,n)}(\theta, l)$ with $\sigma_{(i,j)}(\theta, l)$ if the latter is smaller.

It is not realistic to obtain $\sigma_{\gamma^{(i,j)}}(l)$ based on all $\theta \in [0, 2\pi)$ using Equation 1. Fortunately, due to the spatial redundancy in images, we can obtain an estimate of $\sigma_{\gamma^{(i,j)}}(l)$ using a number of equally spaced θ s. Denote this number to be N_θ and the set of θ s as $\boldsymbol{\theta} = (\theta_1, \dots, \theta_{N_\theta})$. Then Equation 1 becomes

$$\sigma_{\gamma^{(i,j)}}^2(l) = \frac{1}{N_\theta - 1} \sum_{\theta \in \boldsymbol{\theta}} (\gamma^{(i,j)}(\theta, l) - \bar{\gamma}^{(i,j)}(l))^2 \quad (3)$$

and Equation 2 becomes

$$\bar{\gamma}^{(i,j)}(l) = \frac{1}{N_\theta} \sum_{\theta \in \boldsymbol{\theta}} \gamma^{(i,j)}(\theta, l) \quad (4)$$

To make a decision as to whether or not a pixel (i, j) belongs to a line, we first obtain $\gamma^{(i,j)}(l) = \min_{\theta \in \boldsymbol{\theta}} \{\gamma^{(i,j)}(\theta, l)\}$ and $\sigma_{\gamma^{(i,j)}}(l)$. Small $\gamma^{(i,j)}(l)$ and large $\sigma_{\gamma^{(i,j)}}(l)$ indicate the probability of pixel (i, j) belonging to a line, therefore we need to threshold $\gamma^{(i,j)}(l)$ and $\sigma_{\gamma^{(i,j)}}(l)$. First define

$$D(i, j) = \begin{cases} 1 & \text{if } (i, j) \text{ belongs to a line} \\ 0 & \text{otherwise} \end{cases}$$

Then given thresholds T_γ and T_{σ_γ} ,

$$D(i, j) = \begin{cases} 1 & \text{if } \gamma^{(i,j)}(l) < T_\gamma \text{ and } \sigma_{\gamma^{(i,j)}}(l) > T_{\sigma_\gamma} \\ 0 & \text{otherwise} \end{cases}$$

T_γ and T_{σ_γ} are related to the image noise level. In the ideal case, $T_\gamma = 0$ and $T_{\sigma_\gamma} = 0$. As the image gets noisier, both thresholds should be larger.

4 Experimental Results and Discussions

We have described above how a gradient based line detector can fail to extract thick lines. Our proposed line detector can provide better detection in the same test image, including “thin” and “thick” lines. In this section, we will compare the performance of our new technique to that of the compass gradient technique described in Section 2. All the images used in the test were 256×256 with 8 bits per pixel. Our new technique takes about 22, 45, and 90 seconds, respectively, for line detection with $l = 5$, $l = 10$, and $l = 20$ to execute on a SUN Ultra 2 processor.

For the test image shown in Figure 1 (a), the results for the compass gradient approach and our new approach are shown in Figure 2 and Figure 10. To examine the performance of our proposed technique in noisy images, uncorrelated Gaussian noise with mean equal to the graylevel value of the pixels in the lines is introduced in the background of the image in Figure 1 (a). This noisy image has a peak signal-to-noise ratio (PSNR) 14db and is shown in Figure 11 (a). Detection results of the gradient operator and our line detector are shown in Figure 11 (b) and (c), respectively. We can see that the gradient based detector totally missed the lines, while the proposed line detector correctly identified both lines ³.

³It is important to note that Figure 11 (b) does not indicate that the thick line was detected. The black region corresponds to no response from the detector.

Figure 12 illustrates the concept that the parameter l , set *a priori* by the user, corresponds to the maximum width of the lines that will be detected. This feature of our line detector is useful in many applications where one is interested in line features of given widths, for example, the detection of runways in aerial reconnaissance images. The original image is shown in Figure 12 (a), where the top line is 1 pixel wide, the second one is 4 pixel wide, and so on. Each line is 3 pixel wider than the one directly above it. Detection results using $l = 5$, $l = 10$, and $l = 20$ are shown in (b), (c), and (d), respectively. In all cases, lines with width narrower than the l used are detected. While those wider lines are considered as uniform regions.

The same idea can be seen in Figure 13 and Figure 14, where original images are shown in (a) and the corresponding line detection results using $l = 5$, $l = 10$, and $l = 15$, are shown in (b), (c), and (d), respectively. As in Figure 12, only lines with width narrower than the l used are detected. Note also that this line detector responds to both light and dark lines. This can be seen obviously in the upper right section in Figure 13 (d), where lines with different width and graylevels are all detected. This can also be seen in Figure 14 (d), where the black shadow of the car in the lower right section of the image is also detected as lines.

There are many linear structures in digital mammograms, which correspond to shadows of normal ducts and connective tissue elements [19]. It has been shown that suppressing normal background structures enhances the obviousness of abnormal structures [20, 21], which could help radiologists make better decisions regarding the normality of a mammogram. Normal linear structures in mammograms usually appear slightly curved, but over short segments, are approximately linear and have varying thicknesses. These linear structures may have low contrast in a very noisy background. This can be seen in Figure 15 (a), which shows part of a normal mammogram, and Figure 16 (a), which has a cancerous mass in the center. To facilitate line detection, we first lowpass filter the original image, then subtract the result

from the original. This is equivalent to highpass filtering [20, 21]. The enhanced images are shown in Figure 15 (b) and Figure 16 (b), respectively. Our line detector with $l = 20$ is then used on the enhanced images. The detected linear structures are shown in Figure 15 (c) and Figure 16 (c), respectively. We then subtract the detected linear structures from the corresponding enhanced images. Figure 15 (d) and Figure 16 (d) demonstrate that the linear structures are accurately identified and removed from the enhanced mammograms. Also note that the mass in Figure 16 becomes more conspicuous after the linear structures have been removed.

In summary, we proposed a new model for lines and presented a line detection algorithm based on this model. One of the features of our detector is that a user can specify the maximum width of the lines that will be detected. This line detector is also capable of extracting lines with irregular width as well as curves and is robust in the presence of noise. This detector also provides the location of the lines as well as their orientations.

5 Acknowledgments

The authors would like to thank Professor Zygmunt Pizlo of the Department of Psychological Sciences at Purdue University for his helpful suggestions.

REFERENCES

- [1] R. Nevatia and K. Babu, "Linear feature extraction and description," *Computer Graphics and Image Processing*, vol. 13, pp. 257–269, 1980.
- [2] J.-W. Lee and I.-S. Kweon, "Extraction of line features in a noisy image," *Pattern Recognition*, vol. 30, no. 10, pp. 1651–1660, October 1997.
- [3] S. Zucker, R. Hummel, and A. Rosenfield, "An application of relaxation labelling to line and curve enhancement," *IEEE Transactions on Computers*, vol. C-26, no. 4, April 1977.

- [4] Y. Kanazawa and K. Kanatani, "Optimal line fitting and reliability evaluation," *IEICE Transactions on Information and Systems*, no. 9, pp. 1317–1322, September 1996.
- [5] P. H. Eichel, E. J. Delp, K. Koral, and A. J. Buda, "A method for fully automatic definition of coronary arterial edges from cineangiograms," *IEEE Transactions on Medical Imaging*, vol. MI-7, no. 4, pp. 313–320, December 1988.
- [6] G. W. Cook and E. J. Delp, "A gaussian mixture model for edge-enhanced images with applications to sequential edge detection and linking," *Proceedings of the IEEE International Conference on Image Processing*, October 4–7 1998, Chicago, Illinois, pp. 540–544.
- [7] G. W. Cook and E. J. Delp, "Multiresolution sequential edge linking," *Proceedings of the IEEE International Conference on Image Processing*, October 23-26 1995, Washington, DC., pp. 41–44.
- [8] J. Basak, B. Chanda, and D. D. Majumder, "On edge and line linking with connectionist," *IEEE Transactions on Systems, Man and Cybernetics*, vol. 24, no. 3, pp. 413–428, March 1994.
- [9] R. C. Nelson, "Finding line segments by stick growing," *IEEE Transactions on Pattern Analysis and Machine Intelligence*, vol. 15, no. 5, pp. 519–523, May 1994.
- [10] A.-R. Mansouri, A. S. Malowany, and M. D. Levine, "Line detection in digital pictures: a hypothesis prediction/verification paradigm," *Computer Vision, Graphics, and Image Processing*, vol. 40, no. 1, pp. 95–114, October 1987.
- [11] J. B. Burns, A. R. Hanson, and E. M. Riseman, "Extracting straight lines," *IEEE Transactions on Pattern Analysis and Machine Intelligence*, vol. 8, no. 4, pp. 425–455, July 1986.
- [12] A. K. Jain, *Fundamentals of Digital Image Processing*. Prentice-Hall, 1989.
- [13] R. O. Duda and P. E. Hart, *Pattern Recognition and Scene Analysis*. New York: John Wiley, 1973.
- [14] J. Illingworth and J. Kittler, "Survey of the Hough transform," *Computer Vision, Graphics, and Image Processing*, vol. 44, no. 1, pp. 87–116, October 1988.
- [15] H. Koshimizu and M. Numada, "On the extensive reconstruction of Hough-type transform for line pattern detection," *Journal of Information Processing*, vol. 15, no. 2, pp. 243–251, 1992.
- [16] R. C. Agrawal, R. K. Shevgaonkar, and S. C. Sahasrabudhe, "A fresh look at the Hough transform," *Pattern Recognition Letters*, vol. 17, pp. 1065–1068, 1996.
- [17] R. Lo and W. Tsai, "Gray-scale Hough transform for thick line detection in gray-scale images," *Pattern Recognition*, vol. 28, no. 5, pp. 647–661, 1995.

- [18] V. Kamat-Sadekar and S. Ganesan, "Complete description of multiple line segments using the hough transform," *Image and Vision Computing*, vol. 16, no. 9–10, pp. 597–613, July 1998.
- [19] L. W. Bassett, V. P. Jackson, R. Jahan, Y. S. Fu, and R. H. Gold, *Diagnosis of Diseases of the Breast*. W. B. Saunders Company, 1997.
- [20] S. Liu, C. F. Babbs, and E. J. Delp, "Normal mammogram analysis and recognition," *Proceedings of the IEEE International Conference on Image Processing*, October 4–7 1998, Chicago, Illinois, pp. 727–731.
- [21] S. Liu, *The Analysis of Digital Mammograms: Spiculated Tumor Detection and Normal Mammogram Characterization*. PhD thesis, Purdue University, West Lafayette, Indiana, USA, May 1999.

$$\begin{bmatrix} -1 & -1 & -1 \\ 2 & 2 & 2 \\ -1 & -1 & -1 \end{bmatrix} \quad \begin{bmatrix} -1 & -1 & 2 \\ -1 & 2 & -1 \\ 2 & -1 & -1 \end{bmatrix} \quad \begin{bmatrix} -1 & 2 & -1 \\ -1 & 2 & -1 \\ -1 & 2 & -1 \end{bmatrix} \quad \begin{bmatrix} 2 & -1 & -1 \\ -1 & 2 & -1 \\ -1 & -1 & 2 \end{bmatrix}$$

(a) E-W

(b) NE-SW

(c) N-S

(d) NW-SE

Table 1: Compass gradient operators.

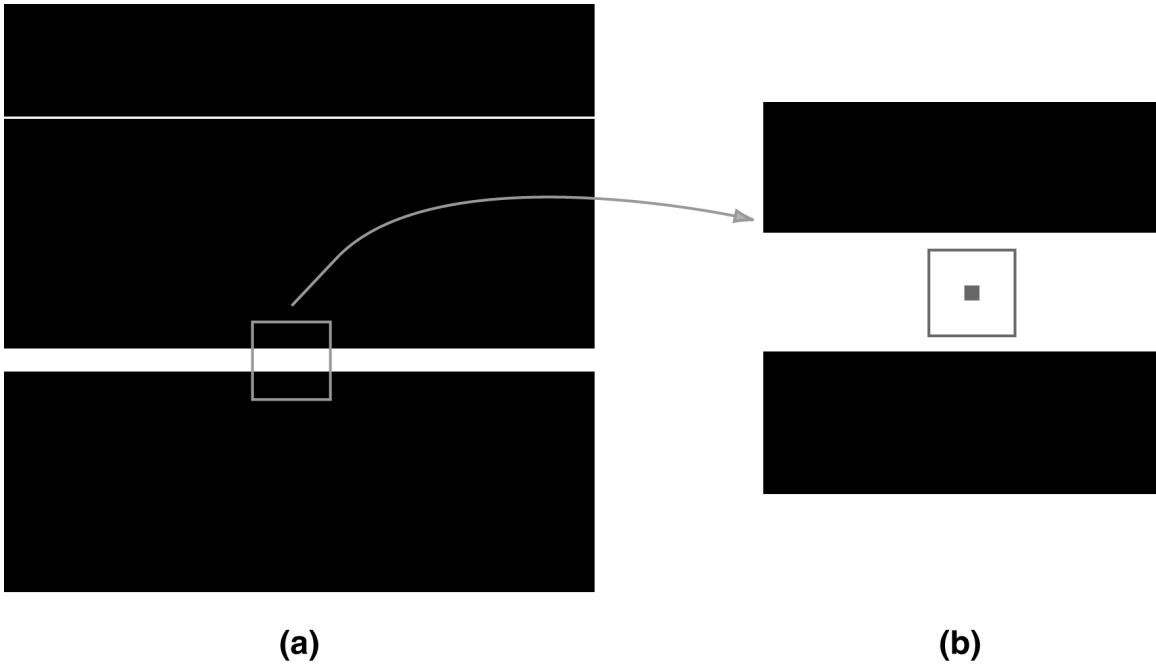


Figure 1: Pixels belonging to a line are not necessarily edge pixels. (a) An image with a 1 pixel wide “thin” white line at the top and a 10 pixel wide “thick” white line at the bottom. (b) The shaded pixel in the middle of the “thick” line looks unlike an edge pixel within a 9×9 neighborhood.



Figure 2: The E-W compass gradient operator detects only edges of the lines in the image shown in Figure 1 (a).

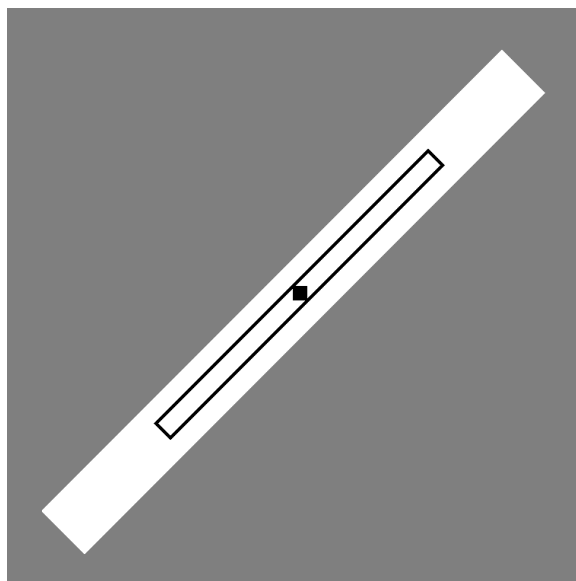


Figure 3: If a pixel belongs to a line, then there exists a string of pixels with similar graylevels along the direction of the line that contains this pixel.

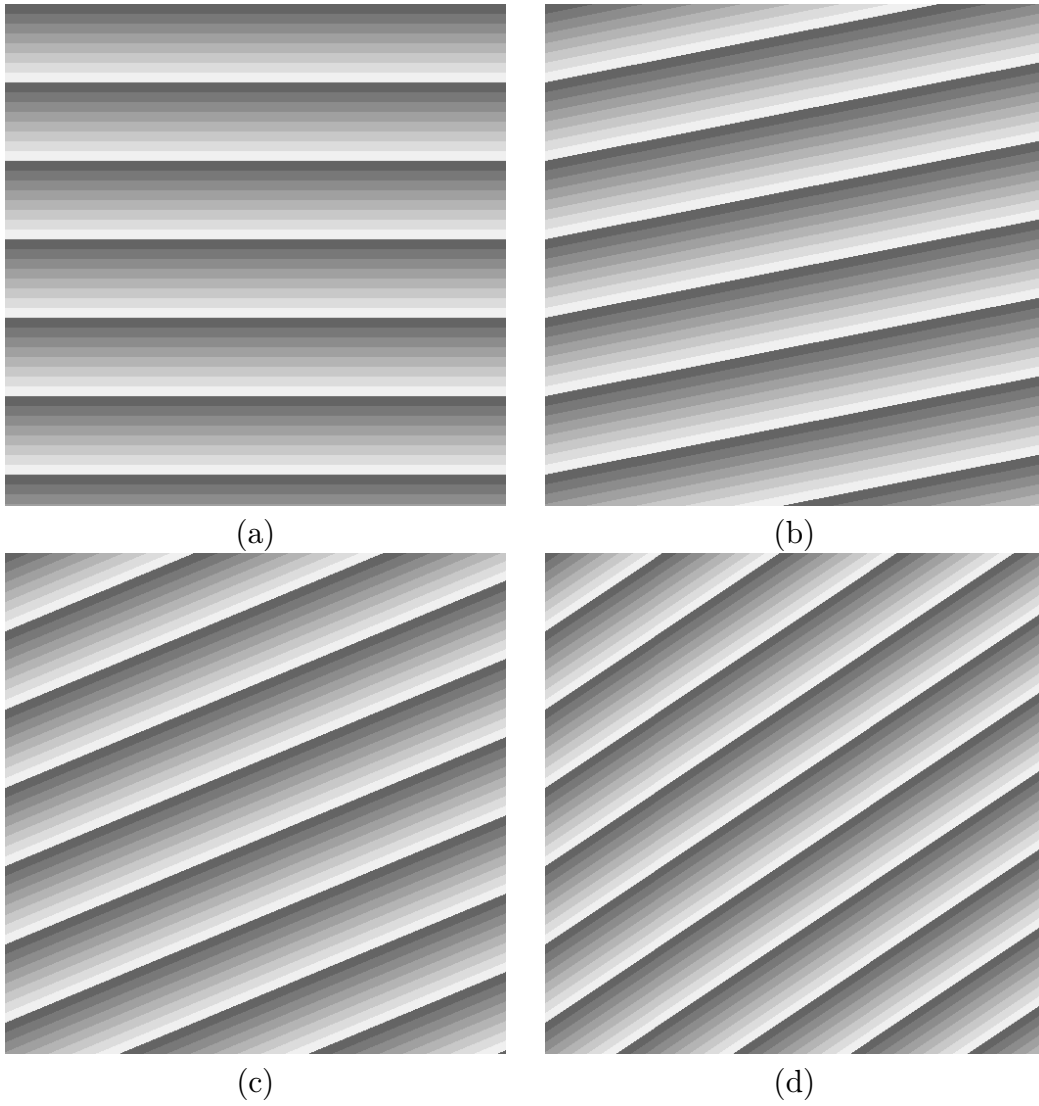


Figure 4: Lines at different orientations (a) 0° . (b) 11.25° . (c) 22.5° . and (d) 33.75° .

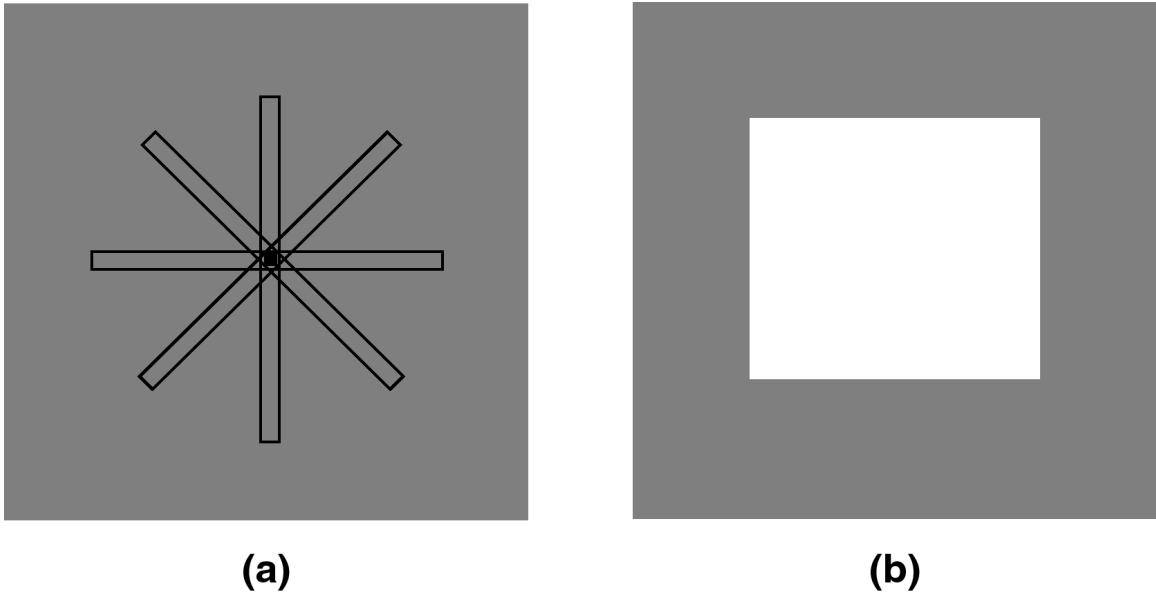


Figure 5: Conditions for a line. (a) The surrounding region has different graylevels from those of the pixels on the line. (b) The length is greater than its width.

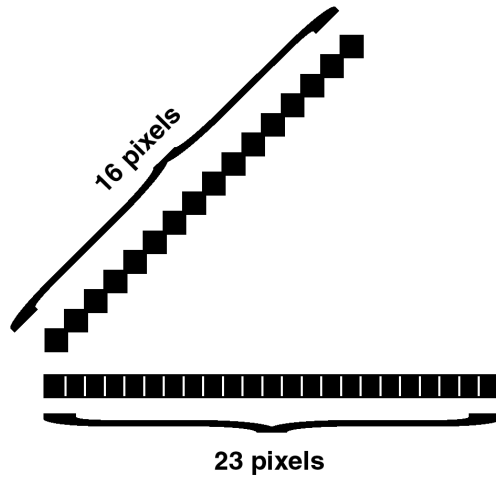


Figure 6: Two strings of the same Euclidean length contain different number of pixels.

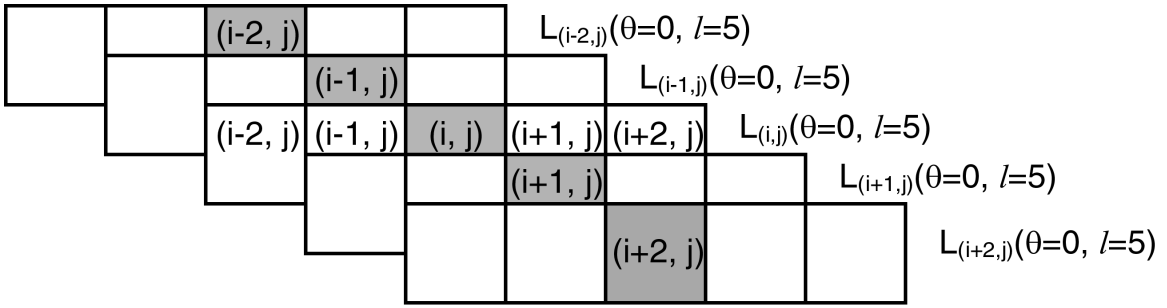


Figure 7: There are $N_{L(\theta,l)}$ number of strings passing through each pixel for given θ and l .

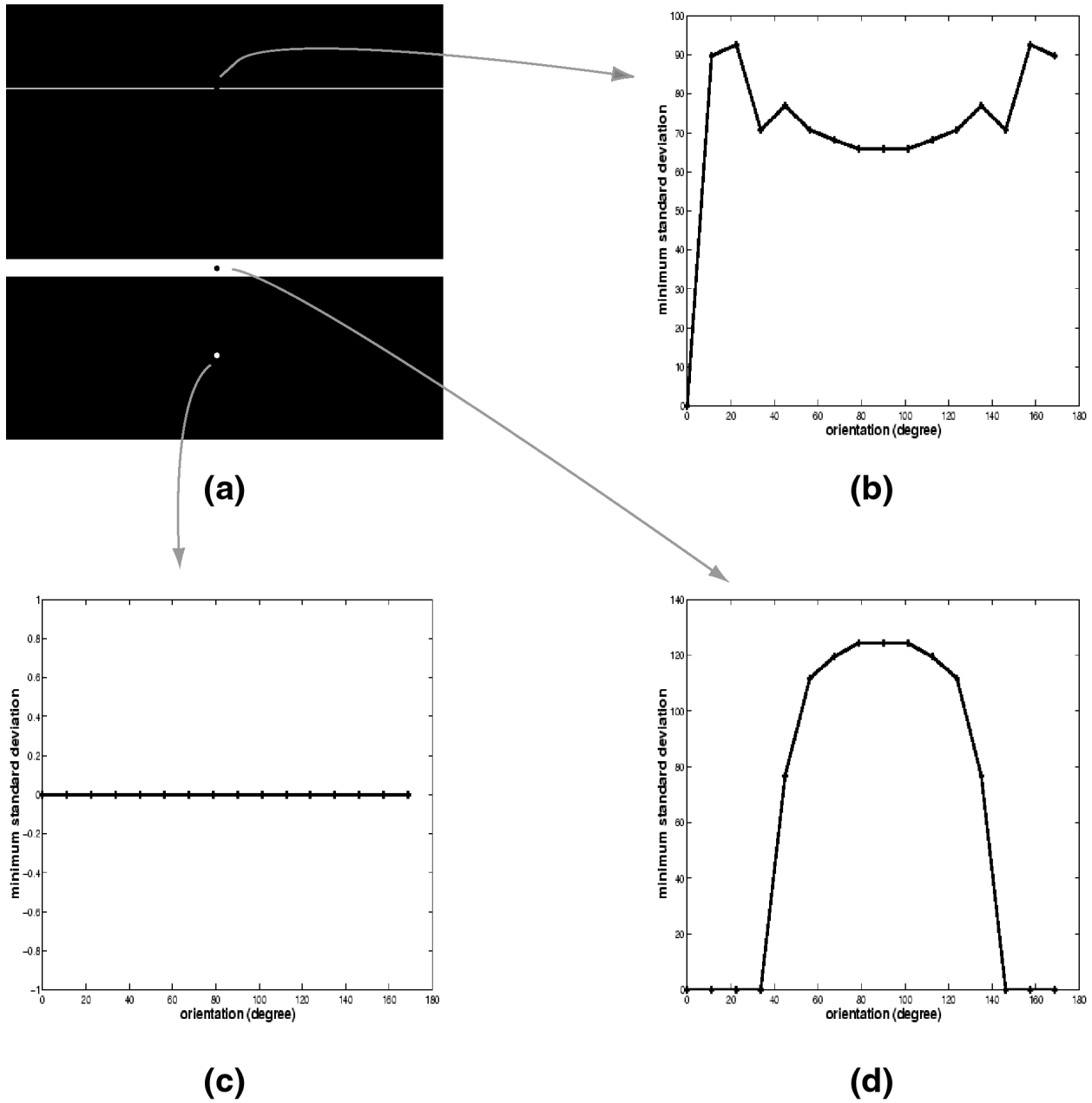


Figure 8: Relationship between $\sigma_{i,j}(\theta, l)$ and θ . (a) Original image. (b) Results for a pixel on the thin line. (c) Results for a pixel in the uniform region. (d) Results for a pixel on the thick line.

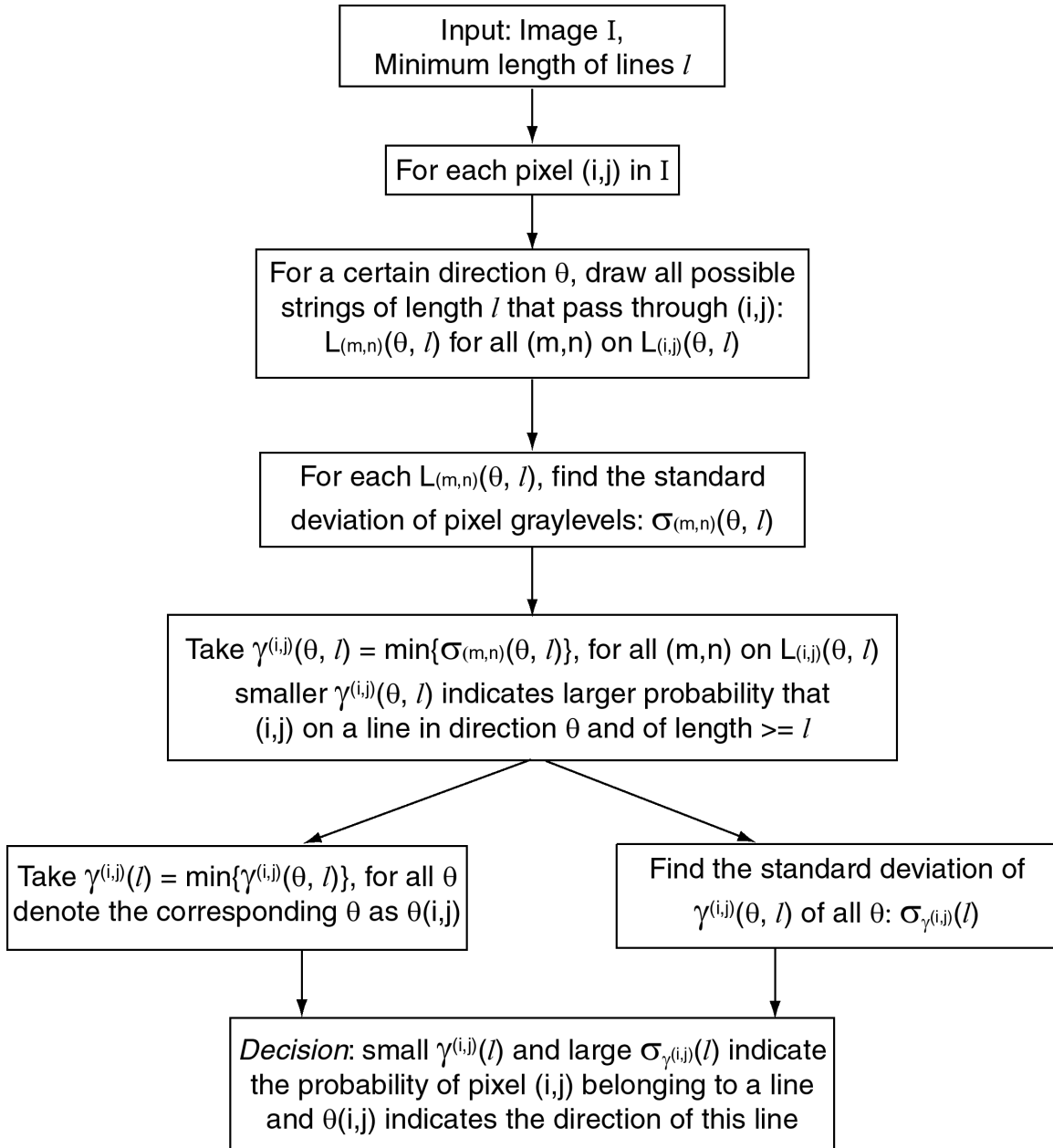
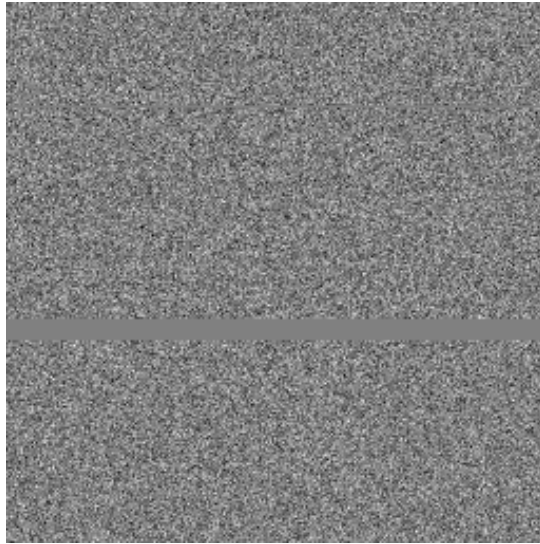


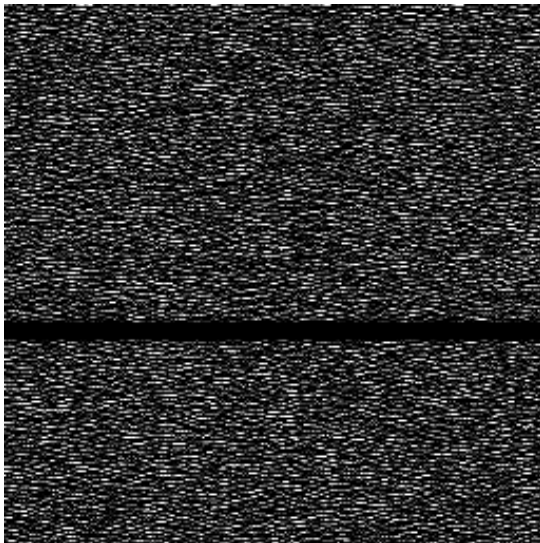
Figure 9: Block diagram of the line detector.



Figure 10: The proposed line detector detects both the “thin” line and the “thick” line in the image shown in Figure 1 (a).



(a)



(b)



(c)

Figure 11: (a) Uncorrelated Gaussian noise with mean the same as that of the lines is introduced to the background of the image in Figure 1 (a), and the peak signal-to-noise ratio (PSNR) is 14db. (b) The E-W compass gradient operator failed to detect the lines. (c) Our proposed line detector correctly identified both lines.

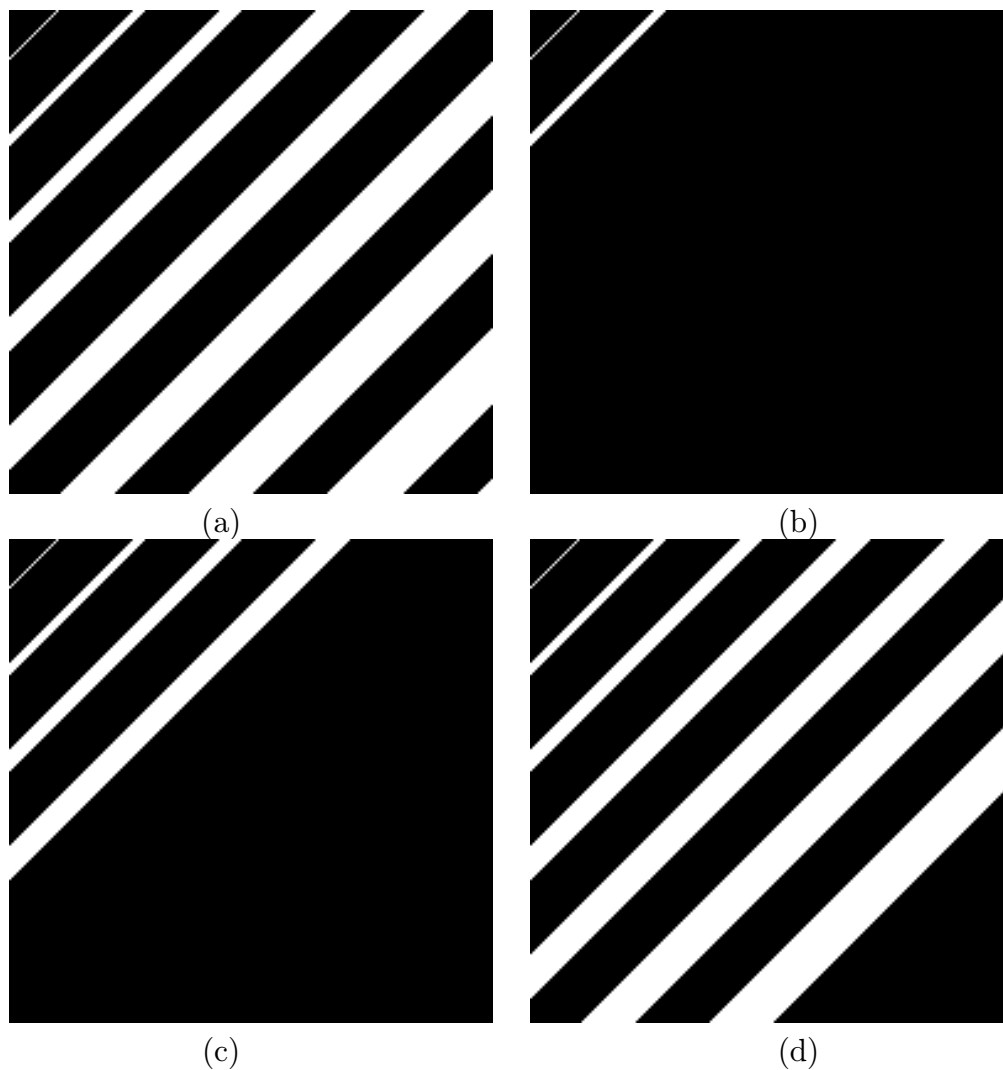
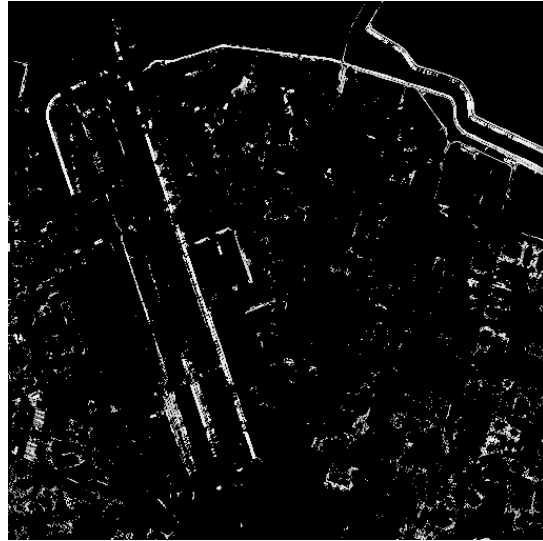


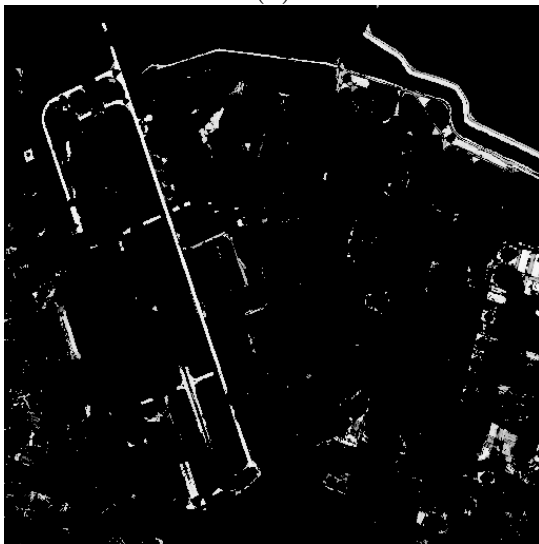
Figure 12: Lines with width narrower than the l chosen are detected, While those wider lines are considered as uniform regions. (a) Original image with the top line 1 pixel wide and each subsequent line is 3 pixel wider than the one directly above it. (b) Detection result using $l = 5$. (c) Detection result using $l = 10$. and (d) Detection result using $l = 20$.



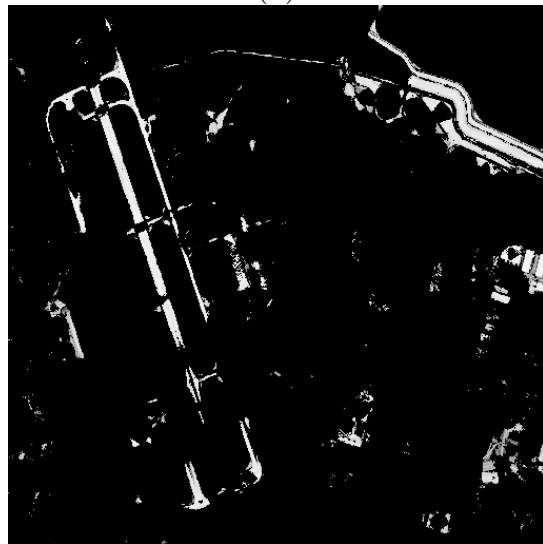
(a)



(b)

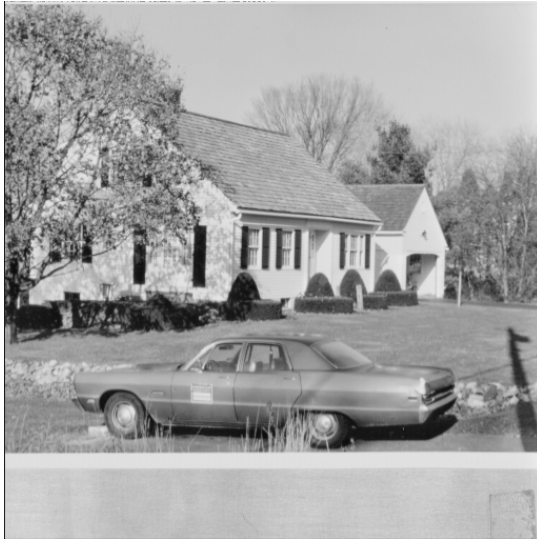


(c)

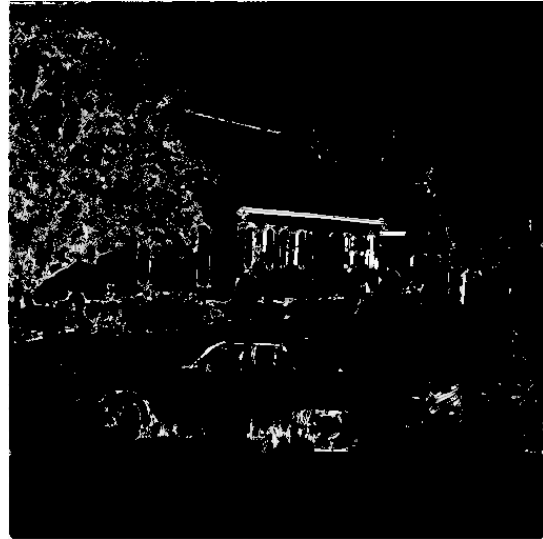


(d)

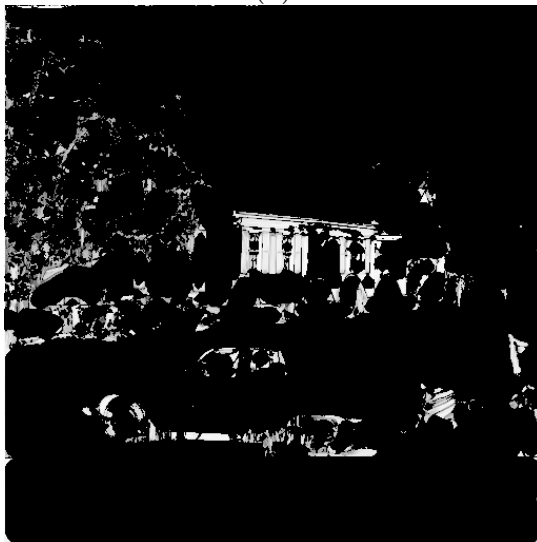
Figure 13: (a) Original aerial image. (b) Detection result using $l = 5$. (c) Detection result using $l = 10$. and (d) Detection result using $l = 15$.



(a)



(b)



(c)



(d)

Figure 14: (a) Original image. (b) Detection result using $l = 5$. (c) Detection result using $l = 10$. and (d) Detection result using $l = 15$.

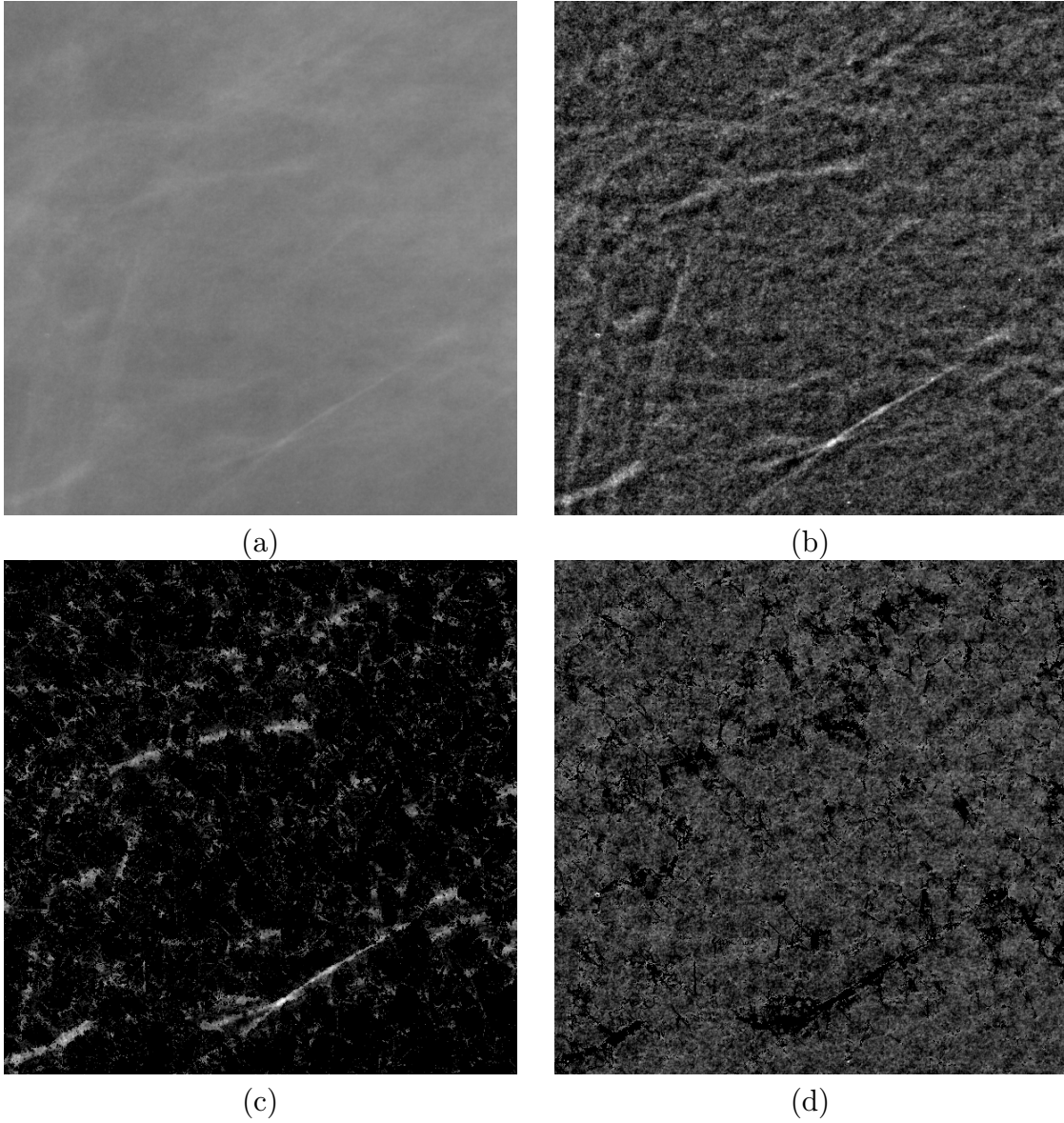


Figure 15: (a) Original normal mammogram. (b) Highpass filtering enhanced image. (c) Linear structures detected from the enhanced image. (d) Removed detected linear structures from the enhanced image.

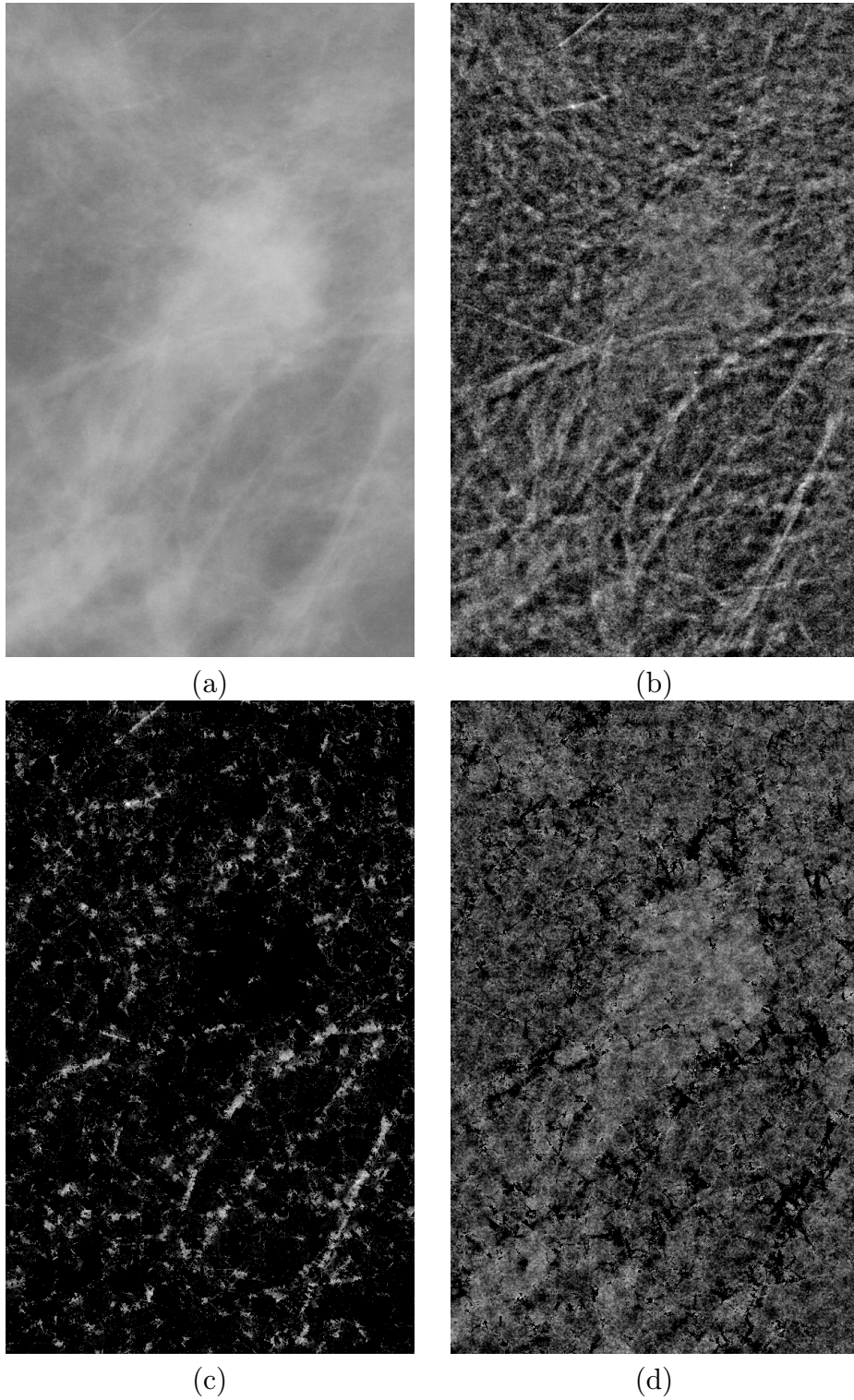


Figure 16: (a) Original mammogram containing circumscribed mass, which is a kind of breast abnormalities. (b) Highpass filtering enhanced image. (c) Linear structures detected from the enhanced image. (d) Removed detected linear structures from the enhanced image and the mass becomes more conspicuous.